Journal of Climate Change
ISSN 2395-7611 Volume 11 (2025) No. 4. pp. 555–568

https://doi.org/10.70917/jcc-2025-036
Article

Aluminium-Based Thermal Management of Lithium–Iron Energy Storage for Sustainable Cooling

Awangku Muhammad Dzul Hisyam [1], Fauziah Jerai[1,2,*], Nor Afifah Yahaya [1] and Norhayati Mat Wajid [1]

[1] Faculty of Mechanical Engineering, Universiti Teknologi MARA, 40450 Shah Alam, Selangor, Malaysia
[2] Wind Engineering & Building Physics (WEBP), Faculty of Mechanical Engineering, Universiti Teknologi MARA, 40450 Shah Alam, Selangor, Malaysia
* Corresponding author: fauziahjerai@uitm.edu.my

Abstract: Climate change represents one of the most pressing challenges of our time, necessitating urgent action across various sectors, including transportation. The transition to electric vehicles is a critical component of this response, offering a pathway to reduce greenhouse gas emissions and promote sustainable mobility. However, the impact of electric vehicles on climate change is closely linked to the lifespan and efficiency of their batteries, which act as energy storage media. As these batteries operate under varying thermal conditions, effective cooling management is essential to optimise their efficiency and ensure safety. Immersion cooling combined with an aluminium casing has emerged as a feasible solution due to its potential for enhanced heat dissipation. Further research is required to understand how aluminium case thickness and cell spacing affect cooling performance with different types of coolants. Therefore, the thermal behaviour of lithium iron phosphate ($LiFePO_4$) battery packs under immersion cooling conditions was analysed in this study using computational fluid dynamics with ANSYS Fluent. The battery cells were encased in aluminium sheets of varying thicknesses and positioned at different intervals. Two types of coolants (pure water and a 40% ethylene glycol (EG)–water mixture) were tested for their effect on temperature regulation and cooling efficiency. The simulation results showed that increasing the thickness of the aluminium casing slightly improved heat dissipation, although the impact was limited at a certain point. Furthermore, larger spacing between cells improved fluid circulation, resulting in a more consistent temperature distribution. The EG–water mixture provided better heat management than pure water, especially at larger casing thicknesses. The optimal configuration for efficient heat management included using a 40% EG–water mixture, a casing thickness of 1.5 mm, and an inter-cell spacing of 40 mm. As a result of these setups, the highest temperature was below 308.00 K and the temperature difference was less than 0.12 K. The results of this research provide useful design suggestions for improving the safety and dependability of $LiFePO_4$ battery systems, in addition to contributing to the current understanding of active thermal management strategies.

Keywords: Lithium iron phosphate; thermal management; computational fluid dynamics; aluminium casing; ethylene glycol coolant

1. Introduction

Climate change has become one of the most critical challenges of our time, affecting ecosystems, meteorological patterns, and global economies. As the world faces escalating temperatures and severe weather occurrences, the demand for sustainable energy solutions becomes ever more urgent (Riffat et al., 2025). The transition to renewable energy systems and electric mobility represents a crucial pathway towards global decarbonisation, with advanced energy storage technologies playing a pivotal role in this transformation (Jarimi et al., 2025). A hopeful direction in the pursuit of cleaner energy is the enhancement and fine-tuning of battery technologies, particularly lithium–iron batteries, which play a

vital role in the transition to renewable energy sources and electric vehicles. The development of efficient thermal management systems for these batteries is essential not only for optimising performance but also for ensuring the long-term reliability and safety of sustainable energy infrastructure (Aydin et al., 2025).

Lithium iron phosphate ($LiFePO_4$) batteries have emerged as a promising solution in modern energy applications, such as in electric vehicles, renewable energy storage systems, and portable electronic appliances (Lin et al., 2021). Their rising popularity is mostly attributed to a combination of advantageous properties, including superior thermal stability, extended cycle life, and relatively high energy density, which make them safer and more durable than other lithium-ion chemistries (Richardson et al., 2021). Operating at a nominal voltage of approximately 3.4 V, $LiFePO_4$ is a safer alternative to other lithium-ion chemistries, such as lithium nickel manganese cobalt oxide, which operates at 3.6–4.2V. This lower operating voltage reduces the risk of thermal runaway, hence improving battery safety (Zeng & Bazant 2014; Zhang et al., 2023).

In order to maintain a good performance of the battery, efficient thermal management is very critical for maintaining battery performance and safety, especially under high power loads. Computational fluid dynamics (CFD) has become a valuable tool in the design and optimisation of battery cooling systems. It allows detailed simulation of heat generation, fluid flow, and temperature distribution across battery modules (Gundran et al., 2019). However, simulation results must be validated through experimental testing under identical conditions and parameters to ensure accuracy and reliability (Gundran et al., 2019; Al-Baghdadi et al., 2020). This integrated approach balances theoretical modelling with practical validation, forming a comprehensive framework for cooling system development.

Material usage in battery thermal management plays a key role. Aluminium is widely utilised due to its high thermal conductivity (200–235 W/m·K), low density, and mechanical strength. Its applications have proven effective in enhancing thermal uniformity, although challenges such as pressure loss and flow resistance necessitate geometry optimisation (Lan et al., 2016). Among the various cooling methods, liquid cooling has demonstrated superior potential for effective battery heat dissipation. Liu et al. (2021) have shown that using aluminium housing with vertically-oriented cooling channels helps reduce temperature gradients across lithium-ion cells. Dambros Telli et al. (2024) employed a parallel flow liquid cooling plate design that improves heat removal while minimising pump energy. Additional innovations include hybrid systems integrating composite silica gel plates (Xu et al., 2021a), dual-channel pathways with nanofluids (Wiriyasart et al., 2020), and thermoelectric cooling using the Peltier effect combined with ferrofluids (Sirikasemsuk et al., 2021a; Sirikasemsuk et al., 2021b). While liquid cooling offers improved performance compared to air-based systems, issues such as coolant leakage and increased system weight still require further optimisation (Situ at al., 2017).

An increasingly promising technique is submerged liquid cooling, in which battery cells are immersed directly in a dielectric fluid to facilitate high-efficiency heat transfer through direct contact. Guo et al. explored the optimisation of multichannel immersion systems by analysing the effects of channel number, flow rate, length, and diameter. Their findings show a highly effective thermal control, with maximum battery temperatures limited to below 309.15 K at a 3C discharge rate. Liu et al. (2023) conducted a numerical study on immersion cooling and found that increasing the coolant flow rate from 0 m/s to 0.35 m/s significantly reduces the maximum temperature rise by 63%, from 284.13 K to 277.72 K. Despite these advantages, submerged cooling systems present challenges such as fluid compatibility, risks of leakage, and system complexity. However, their ability to achieve uniform temperature distribution and maintain optimum operating temperatures makes them a highly attractive solution. Although the advantages of immersion cooling are becoming more widely acknowledged, comprehensive research incorporating aluminium casing into immersed $LiFePO_4$ battery pack cooling is still lacking. Specifically, the influence of aluminium casing thickness and inter-cell spacing on thermal performance remains underexplored.

This study aims to investigate an efficient submerged liquid cooling thermal management solution for $LiFePO_4$ battery packs, focusing on the application of CFD analysis. It integrates an aluminium casing and varies the coolant type, the spacing between cells, and the casing thickness, as part of developing a safe and compact battery thermal solution.

2. Methodology

This section describes the methodology employed to analyse the thermal performance of a submerged liquid cooling system for prismatic $LiFePO_4$ battery cells. The methodology includes the development of models, meshing strategy, simulation setup, solver setup, boundary conditions, post-processing techniques, and validation procedures. A numerical simulation was performed using ANSYS Fluent under transient settings to investigate heat dissipation utilising various coolants. The process began with

the development of a simplified three-dimensional (3D) geometry of a four-cell battery module, followed by meshing, specification of material and coolant properties, application of boundary conditions, and performing thermal-fluid analysis over time. A structured study was conducted to examine the effects of coolant type, aluminium casing thickness, and inter-cell spacing on thermal performance.

2.1. Governing Equations

The thermal and fluid dynamics behaviour of the battery cooling system was modelled using the fundamental conservation laws of mass, momentum, and energy, as shown in Table 1. The coolant flow was represented as a 3D, incompressible, laminar flow with constant fluid properties. Heat generation within the battery cell was assumed to be uniformly distributed across the active region. The following equations were used in the simulation (Omar & Adham et al., 2025; Xu et al., 2021b).

Table 1. Governing Equations.

Name	Equation	Equation No.
Continuity	$\frac{\partial u_i}{\partial x_i} = 0$	(1)
Navier-Stokes Equation (Momentum Equation)	$\rho_a \frac{\partial u_i}{\partial t} + \rho_a u_j \frac{\partial u_i}{\partial x_j} = - \frac{\partial p}{\partial x_i} + \frac{\partial}{\partial x_j} (\mu + \mu_t) \frac{\partial u_i}{\partial x_j}$	(2)
Energy Conservation of Lithium Battery Pack	$\rho_c C \frac{\partial T}{\partial t} = k \left(\frac{\partial^2 T}{\partial x^2} + \frac{\partial^2 T}{\partial y^2} + \frac{\partial^2 T}{\partial z^2} \right) + Q$	(3)
Energy Conservation of Casing	$\rho_p C_p \frac{\partial T_p}{\partial t} = \nabla \cdot (k_p \nabla T_p)$	(4)
Energy Conservation of Coolant	$\rho_c C_c \frac{\partial T_c}{\partial t} = \nabla \cdot (k_c \nabla T_c)$	(5)
Convective Heat Transfer	$q = h(T_C - T_0)$	(6)

2.2. Geometry Configuration

The geometric model was developed to represent the physical configuration of the $LiFePO_4$ battery pack, aluminium casing, and the surrounding coolant area in a simplified yet realistic manner. The key objective was to capture the essential elements affecting heat generation, conduction, convection, and heat removal, while ensuring the model remained compatible with simulation. The complete geometry including the inlet/outlet locations, individual battery cells, and casing was created and developed using SolidWorks 2024 (Figure 1), which was then converted and imported into ANSYS Fluent. The geometry was examined for gaps and overlaps that could compromise meshing quality. The key dimensions of the battery cells, casing, and coolant domain are summarised in Table 2.

Table 2. Dimensions of the Battery and Coolant Domains.

Component	Parameter	Value (mm)
Battery Cell	Length	157
Battery Cell	Height	144
Battery Cell	Thickness	28
Inter-Cell Spacing	Tested values	20/30/40
Casing	Thickness	1.5/2.0/2.5
Domain	Height	140
Domain	Width	242
Domain	Length	331
Inlet/Outlet	Opening size	50 × 30 × 10

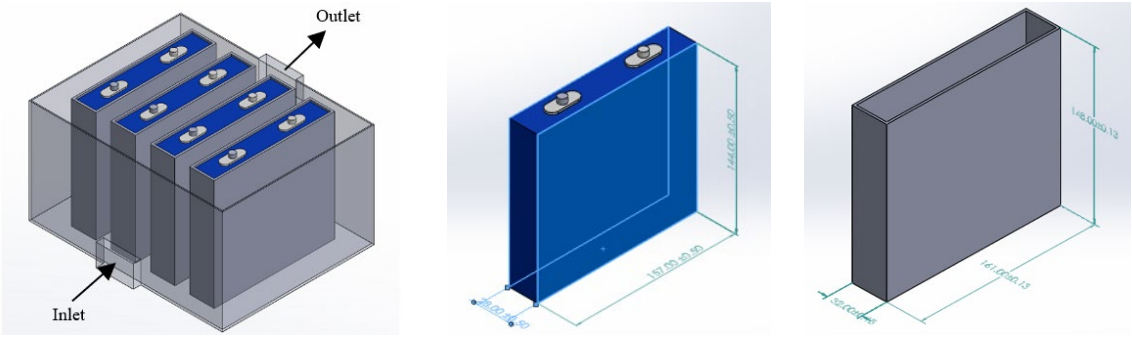

(a) **(b)** **(c)**

Figure 1. Geometry and Domain Setup: (**a**) Inlet and Outlet Locations, (**b**) Battery Cell, and **(c)** Casing Geometry.

2.3 Meshing and Grid Independence Study

The 3D model was meshed using structured tetrahedral elements. A fine mesh was used to accurately capture heat transfer and temperature gradients, as shown in Table 3. A grid independence test was performed by comparing the optimal balance between accuracy and runtime. The meshing comprising 521,310 elements was selected as the optimal balance between accuracy and runtime (Figure 2). A slight non-monotonic increase in maximum temperature was observed between the coarse and intermediate mesh sizes. This increase reflects the improved resolution of localised temperature gradients as the mesh is refined, as coarser grids tend to underpredict convective and conductive heat transfer near solid–fluid interfaces. At finer mesh sizes, the spatial resolution of isolated hotspot zones improves, allowing the solver to more precisely capture strong gradients near cell interfaces, resulting in a higher but physically realistic maximum temperature. Once the element count exceeded approximately 500,000, the results stabilised, confirming mesh independence and numerical consistency.

Table 3. Grid Independence Study.

Element Size (mm)	Total Elements	Maximum Temperature (K)
0.0050	150,386	140.01
0.0040	226,126	189.37
0.0035	**521,310**	300.87
0.0030	727,753	300.87
0.0025	1,032,836	300.82

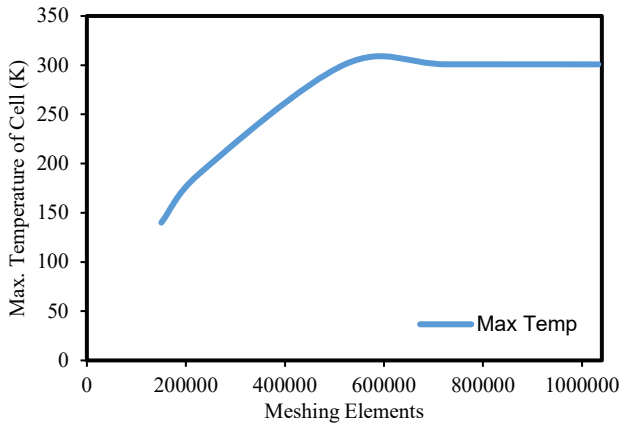

Figure 2. Grid Independence Study.

2.4. Material Properties

The thermophysical properties for the entire domain were assumed to be constant and consistent within the typical operating temperature of the battery. These properties include the density, thermal conductivity, and specific heat capacity of the battery cells and casing, as well as the viscosity of the coolant. As shown in Table 4, a 40% ethylene glycol (EG)–water mixture was selected as the coolant due to its ability to lower the freezing point of water to approximately 233.15 K, making it suitable for use in heat exchangers and engine cooling systems (Syam Sundar & Shaik, 2023).

2.5. Boundary Conditions

Heat generation in $LiFePO_4$ battery cells was modelled to represent the thermal load during discharge. In this study, each cell was assumed to be discharged at a rate of 3C, which is a high current condition commonly used to evaluate thermal performance. Higher discharge rates generate more internal heat due to increased electrical losses. The total heat generation is calculated using the Bernardi equation, which considers both irreversible and reversible heat generation mechanisms (Wang et al., 2024). The chosen heat generation rate of 30,237 W/m^3 corresponds to a 3C discharge rate, replicating the high-load conditions commonly found in electric vehicles and energy-intensive applications (Hemavathi et al., 2024). While the outlet conditions ensure realistic flow dynamics, the coolant inlet was assigned a specific temperature of 298.15 K and velocity profiles. The aluminium casing walls were subjected to non-slip conditions to simulate the coolant-surface interaction (Duan et al., 2021). To evaluate their effect on cooling performance, simulations were conducted with a mass flow rate set at 0.005 kg/s. A pressure outlet boundary condition was applied at the outlet face, allowing the coolant to exit freely while maintaining a stable pressure profile. The gauge pressure was set to 0 Pa, representing discharge to atmospheric conditions.

Table 4. Thermophysical Properties.

Material	Density (kg/m^3)	Thermal Conductivity (W/m·K)	Specific Heat (J/kg·K)	Viscosity (kg/m·s)	Reference
Aluminium	2,719.00	202.40	871.00	-	-
40% EG–Water Mixture	1,056.72	0.4096	3,491.80	0.00245	(Idris et al., 2024)
Water	998.20	0.60	4,182.00	0.001003	-

2.6. Simulation Scenarios

Two phases of simulation were designed to fulfil the objectives of the study, as shown in Table 5 and Table 6. Phase 1 involves coolant evaluation to identify the best coolant using constant thickness and spacing. Phase 2 focuses on geometric optimisation, assessing how variations in geometry affect cooling when using the best coolant identified in Phase 1.

Table 5. Phase 1: Coolant Evaluation.

Case	Coolant Type	Casing Thickness (mm)	Cell Spacing (mm)
A1	Water	2.0	20
A2	EG–Water (40:60)	2.0	20

Table 6. Phase 2: Geometric Optimisation.

Case	Casing Thickness (mm)	Spacing between Cells (mm)	Coolant Type
B1	1.5	20	EG–Water (40:60)
B2	1.5	30	EG–Water (40:60)
B3	1.5	40	EG–Water (40:60)
C1	2.0	20	EG–Water (40:60)
C2	2.0	30	EG–Water (40:60)
C3	2.0	40	EG–Water (40:60)
D1	3.0	20	EG–Water (40:60)
D2	3.0	30	EG–Water (40:60)
D3	3.0	40	EG–Water (40:60)

2.7. Post-Processing

This section involves extracting, interpreting, and analysing simulation results to evaluate the cooling performance of the submerged thermal management system. The goal is to quantify temperature distribution, identify thermal hotspots, and assess temperature uniformity. A summary of the post-processing metrics and measurement points is presented in Figure 3 and Table 7.

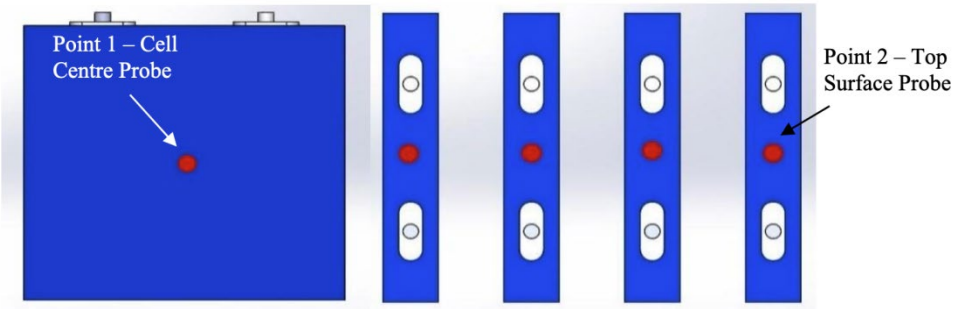

Figure 3. Measurement Points.

Table 7. Summary of Post-Processing Metrics and Measurement Points.

Category	Metric	Description
Primary Evaluation Metrics	Maximum cell temperature	Identify the peak thermal zones
	Minimum cell temperature	Measure the lowest temperature of the cell
	Average cell temperature	Represents the overall thermal condition of the cell
	Temperature gradient between cells	Evaluate temperature uniformity
Measurement Points	Point 1: Cell centre	Captures core heating temperature
	Point 2: Cell's top surface	Detects surface-level temperature

3. Results and Discussion

This section summarises the results of the CFD analysis performed on a prismatic $LiFePO_4$ battery pack under different cooling arrangements. The simulations were designed to assess the thermal performance of two coolant types: pure water and a 40% EG–water mixture, followed by geometry-based optimisation of casing thickness and inter-cell spacing using the better-performed coolant. All simulations were transient, with a discharge rate of 3C and a discharge duration of 600 s for each case.

3.1. Raw Simulation Results

The visualisation of thermal and flow behaviour helps to clarify how heat and fluid move through a system. Thermal contours illustrate the temperature distribution, showing hotspots, while flow streamlines indicate how coolant flows, indicating zones with high and low flow. These insights provide data on system efficiency and can be useful for potential enhancements to achieve optimal cooling.

Figure 4 (a)–(d) illustrate the visualisation of the model's flow behaviour. Figure 4 (a) presents the top view, providing a clear view of flow uniformity across the cell surface and highlighting the distribution of cooling between cells. Figure 4 (b) shows the isometric view of the flow, demonstrating how heat is efficiently carried away from the casing. Figure 4 (c) displays the temperature pattern of the battery casing, with concentrated red regions indicating warmer temperatures compared to the surrounding areas. This suggests that heat has accumulated at the centre of the casing, most likely as a result of internal battery operation at the centre of the cell. The temperature distribution inside the battery cells is depicted in Figure 4 (d). The red region at the centre of the cells exhibits the highest temperature, implying that the cell's core produces greater heat during operation due to internal chemical reactions. The colder regions near the edges, represented in green and blue, indicate less heat buildup, owing to the effect of the cooling system.

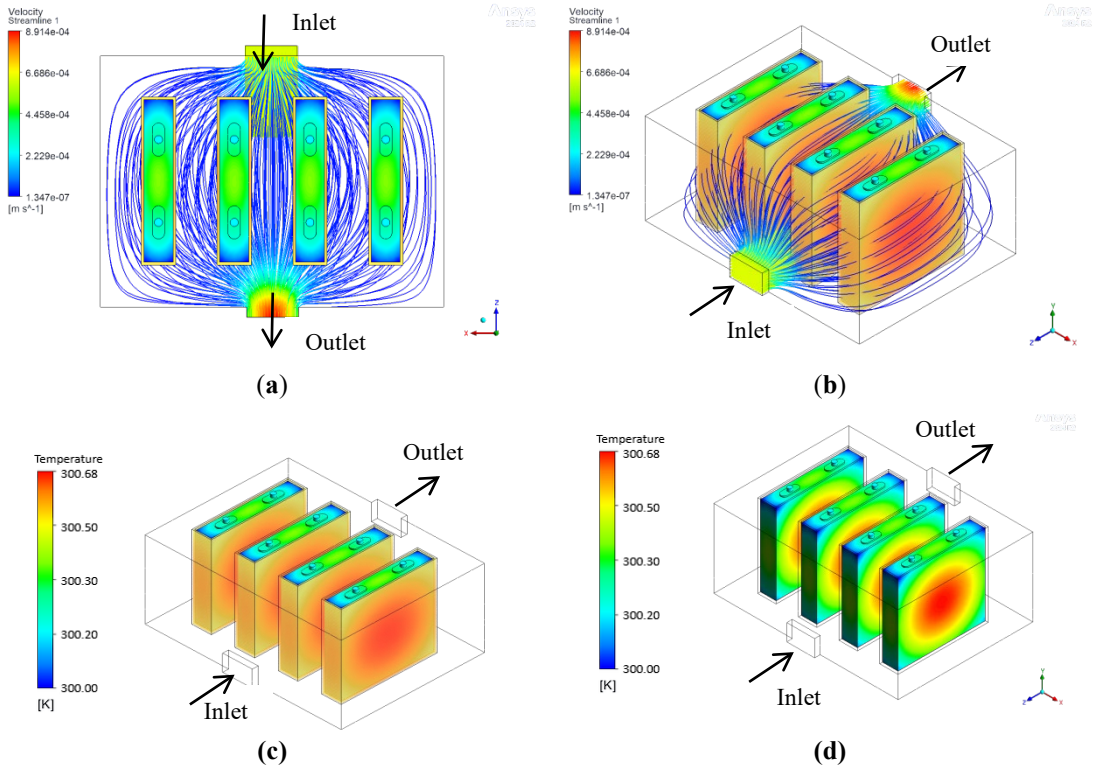

Figure 4. Visualisation of Thermal and Flow Behaviour: (**a**) Top View of the Flow, (**b**) Isometric View of the Flow, (**c**) Casing Temperature Distribution, and (**d**) Cell Temperature Distribution.

3.2. Quantitative Performance Metrics

This section examines the cooling performance of two types of coolant: pure water and a 40% EG–water mixture under submerged cooling. The impact of coolant parameters, such as thermal conductivity and specific heat capacity, on overall thermal management was assessed through the analysis of maximum cell temperature and thermal trends, as shown in Table 8. This comparison aids in selecting the best coolant for battery pack cooling.

Table 8. Temperature Distribution.

Coolant Type	Max. Temp (K)	Min. Temp (K)	ΔT (K)
Pure Water	300.62	300.50	0.12
40:60 EG–Water Mixture	300.63	300.50	0.13

Figure 5 shows the maximum and minimum temperatures of battery cells cooled with pure water and a 60:40 EG–water mixture. Both coolants exhibit great thermal control, with temperature differences (ΔT) of 0.12 K and 0.13 K, respectively. The EG–water mixture exhibits a slightly higher maximum temperature (300.63 K) than pure water (300.62 K), indicating a small but noticeable variation in thermal control capabilities. Although the EG–water mixture has a slightly higher maximum temperature, the difference in performance is negligible (only 0.01 K in practical terms). The increased viscosity of the EG–water mixture may have resulted in a slight reduction in convective heat transfer, explaining the higher maximum temperature. However, this small variance has no substantial impact on overall cooling performance, especially given the great temperature uniformity and steady profile observed throughout the discharge cycle. The findings indicate that both coolants can sustain stable thermal conditions, although the EG–water mixture may be more suitable for scenarios where boiling point elevation, thermal stability, and long-term dependability are prioritised over marginal temperature reductions. This could result in increased safety margins and more consistent thermal performance across a wide range of ambient temperatures in high-load applications.

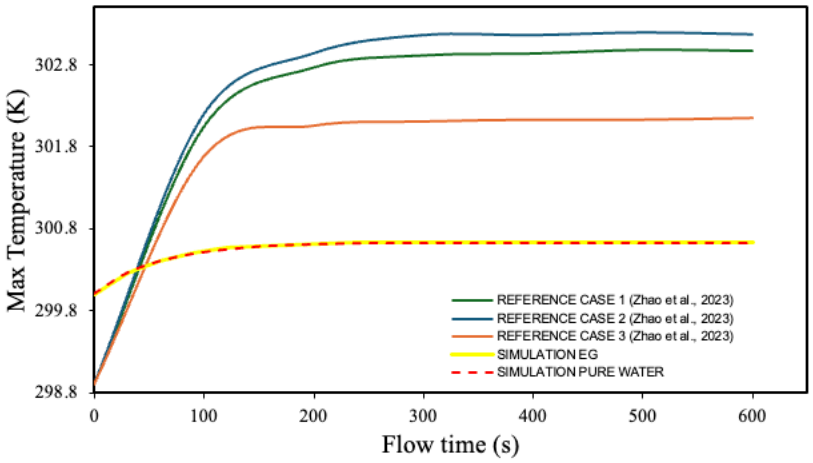

Figure 5. Maximum Cell Temperature of Different Coolants with Reference to Maximum Temperature over Time.

This comparison used a single flow rate (0.005 kg/s) with an initial coolant temperature of 298.00 K. The slight temperature difference observed may vary depending on the flow conditions, discharge rates, and coolant composition. Furthermore, this study did not evaluate the implications of long-term coolant degradation or the possible corrosion issues associated with glycol mixtures. As shown in Figure 5, both coolant types experience a temperature rise during the initial simulation period, followed by temperature stabilisation after approximately 240 s. Research on liquid cooling plates for prismatic $LiFePO_4$ cells found that the maximum temperature increased and stabilised around 300 s. This pattern suggests that the system has reached thermal equilibrium, which is a common occurrence in battery thermal behaviour under constant heat generation. To validate this finding, Figure 5 includes a reference from Zhao et al., (2023), who reported a comparable temperature response. The close agreement between the present simulation and published reference cases serves as a form of validation, reinforcing the reliability of the numerical predictions.

The effectiveness of the cooling system in removing heat from battery cells during 3C discharge was also assessed. Cooling efficiency was measured by dividing the amount of heat removed by the coolant by the total heat generated within the battery module. The heat generation rate for each cell was calculated to be 30,237 W/m^3, based on the provided values of $LiFePO_4$ batteries. According to Figure 6, water achieved a cooling efficiency of 70.12%, whereas a 40% EG–water mixture obtained 58.56%. Although both coolants efficiently removed the generated heat, water's higher efficiency is attributable to its superior thermal characteristics. Understanding cooling efficiency is critical in the design of a real-world battery system. A system with inadequate efficiency may experience heat accumulation, limiting the lifespan and increasing the risk of thermal runaway. This analysis assumed uniform heat generation across all cells; however, in practical applications, heat generation could vary over time and location.

Table 9. Phase 1: Heat Transfer Rates for Different Coolants.

Coolant Type	Inlet Temperature (K)	Heat Transfer Rate (W)
40% EG–Water Mixture	298.15	44.82
Pure Water	298.15	53.67

Table 9 compares the heat transfer performance of a 40% EG–water mixture with that of pure water at the same inlet temperature of 298.15 K. The results indicate that pure water removed more heat (53.67 W) compared to the EG–water mixture (44.82 W). This difference can be attributed to the superior thermal conductivity and specific heat capacity of water relative to EG. While the addition of EG enhances coolant stability and lowers the freezing point, making it more suitable for practical applications under varying environmental conditions, it also reduces the overall heat transfer efficiency due to its lower thermal properties. Although pure water provides superior heat transfer performance, the EG–water mixture offers a balance between thermal efficiency and operational reliability, particularly in scenarios where freezing protection and long-term stability of the coolant are critical.

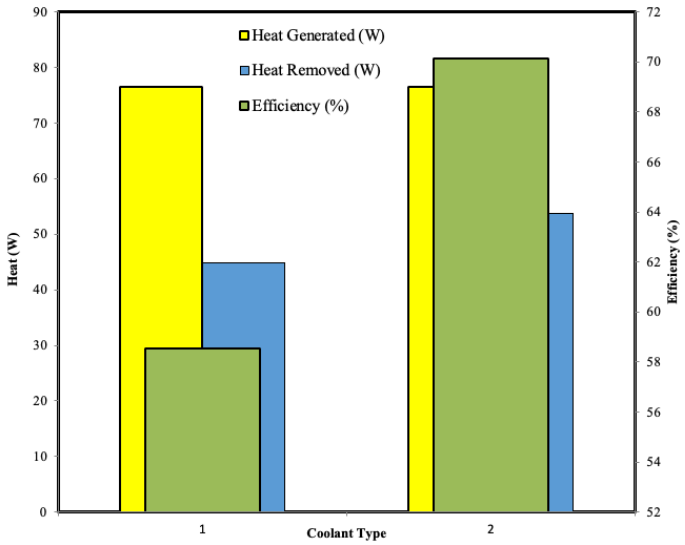

Figure 6. Comparison of Heat Generation, Heat Removal, and Cooling Efficiency.

3.3 Results of the Parametric Analysis

3.3.1. Effect of Aluminium Casing

Figure 7 illustrates the effect of the aluminium casing on the battery's maximum cell temperature over time. Without a casing, the temperature rises steadily, reaching 301.09 K. With the aluminium casing, the cell temperature stabilises around 300.62 K, which is notably lower. The data demonstrates the aluminum enclosure's positive effect on temperature control as a 0.50 K reduction in peak temperature can be critical in preventing thermal runaway under extreme conditions. Therefore, the incorporation of aluminium as a passive heat spreader offers a cost-effective and practical design improvement for thermal management systems in electric vehicles and stationary energy storage.

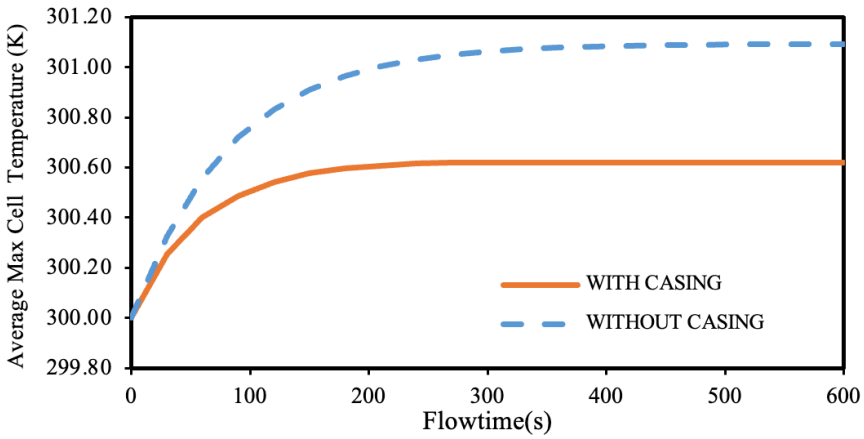

Figure 7. Maximum Cell Temperature With and Without Aluminium Casing.

3.3.2. Effect of Casing Thickness

Heat dissipation was tested using three different casing thicknesses: 1.5, 2.0, and 2.5 mm. The casing acts as a thermal barrier between the cells and the coolant. The thickness influences the efficiency of heat transfer from the cells to the coolant.

Figure 8 (a) shows the correlation between casing thickness and the maximum temperature at Point 1. The data indicate a noticeable rise in temperature as the casing thickness increases from 1.5 to 2.5 mm. At 1.5 mm thickness, the maximum temperature is approximately 300.593 K, whereas at 2.5 mm, it increases to 300.676 K. This suggests that, although increasing casing thickness enhances heat dissipation capacity, its effect on temperature control is minimal. The gradual rise in temperature implies a reduction in heat dissipation efficiency as thickness increases, emphasising that coolant properties and flow dynamics are likely to play a more significant role in overall heat management. Figure 8 (b) displays

the ΔT between the maximum and minimum temperatures within each cell for different casing thicknesses. At 1.5 mm thickness, there is a large ΔT variation, particularly in Cell 4, where the ΔT reaches 0.232 K. This indicates increased thermal instability or less effective heat distribution. As the casing thickness increases to 2 and 2.5 mm, ΔT values decrease to between 0.111 K and 0.129 K, indicating improved thermal uniformity. This suggests that thicker casings help reduce temperature variance within individual cells, most likely due to improved thermal conduction and heat distribution. Analysing ΔT is crucial because large temperature fluctuations within cells can cause thermal stress and degradation. Increased thickness reduces ΔT, thus improving thermal stability.

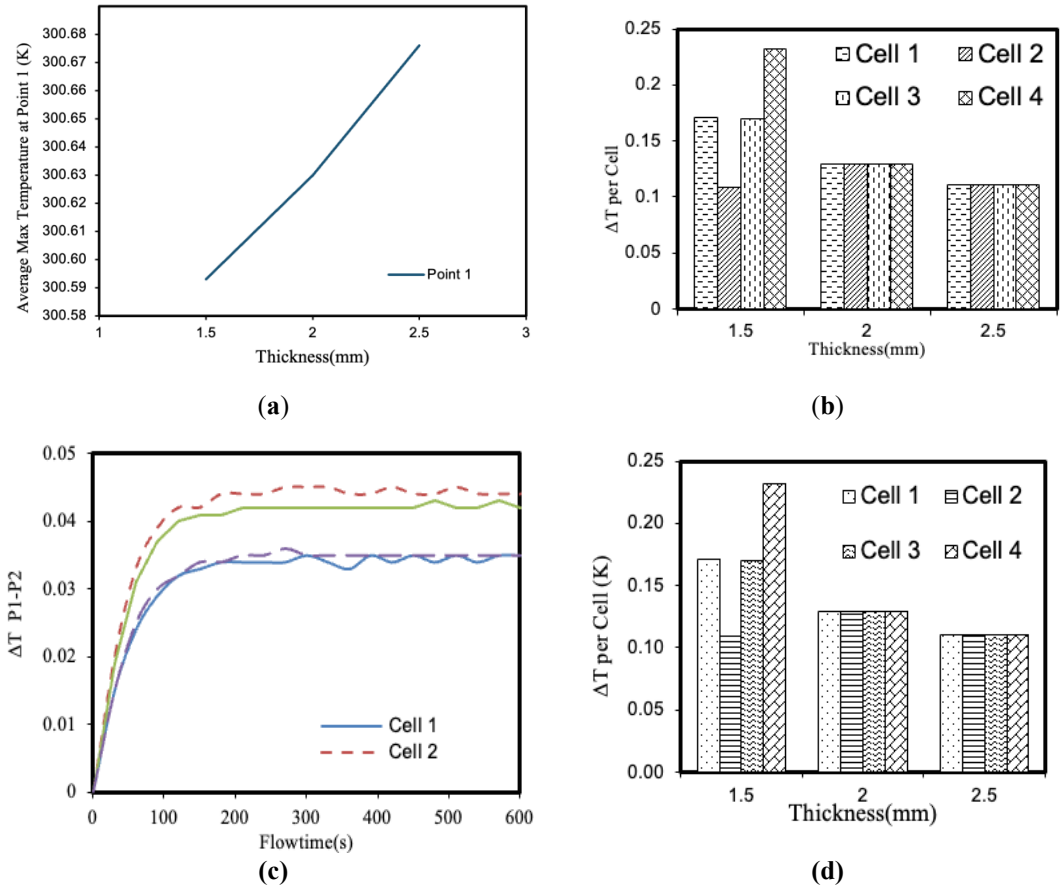

Figure 8. Effect of Casing Thickness: **(a)** Maximum Temperature versus Thickness, **(b)** Temperature Difference Per Cell versus Thickness, **(c)** Temperature Difference between P1 and P2 at 1.5 mm Thickness versus Flowtime, and **(d)** Temperature Difference Per Cell at Different Casing Thicknesses.

Figure 8 (c) visualises the vertical thermal gradient (ΔT between the centre and top) for each cell over time. The data show that Cell 1 has the lowest gradient (ΔT ranging from 0.015 K to 0.035 K), indicating efficient vertical heat transfer. Cells 2 and 3 exhibit significantly greater gradients (ΔT of up to 0.045 K), suggesting inefficient heat transfer. Cell 4 has the largest gradient, with ΔT reaching up to 0.045 K, indicating poor vertical heat distribution. Analysing the P1–P2 gradient is important because it reveals how heat flows vertically within the cell. The higher gradient in Cell 4 highlights thermal management concerns that could lead to uneven heating, thereby reducing battery efficiency and lifespan. Figure 8 (d) shows the results of using different thicknesses with a constant inter-cell spacing of 30 mm. Increasing the casing thickness from 1.5 mm to 2.5 mm decreases the average ΔT across the cell from 0.1705 K to 0.1110 K, suggesting improved thermal uniformity. Although the maximum temperature increased, the reduction in ΔT shows that a thicker casing diffuses heat more uniformly and minimises localised hotspots. The 2.5 mm thickness provides better temperature consistency without severe thermal effects. In summary, increasing the casing thickness from 1.5 mm to 2.5 mm results in a slight rise in maximum temperature and ΔT, with the primary benefit being enhanced thermal uniformity and lower vertical heat gradients across cells. Thicker casings help to transfer heat evenly, minimising thermal stress and promoting more consistent cooling throughout the battery pack. However, the small increase in

temperature suggests that other factors, such as coolant properties, flow rates, and cell design, have a greater impact on overall cooling performance.

3.3.3. Effect of Inter-Cell Spacing

A series of spacing measurements, specifically 20, 30, and 40 mm, was employed to assess whether increasing the spacing would improve coolant access and thermal equilibrium within the cells.

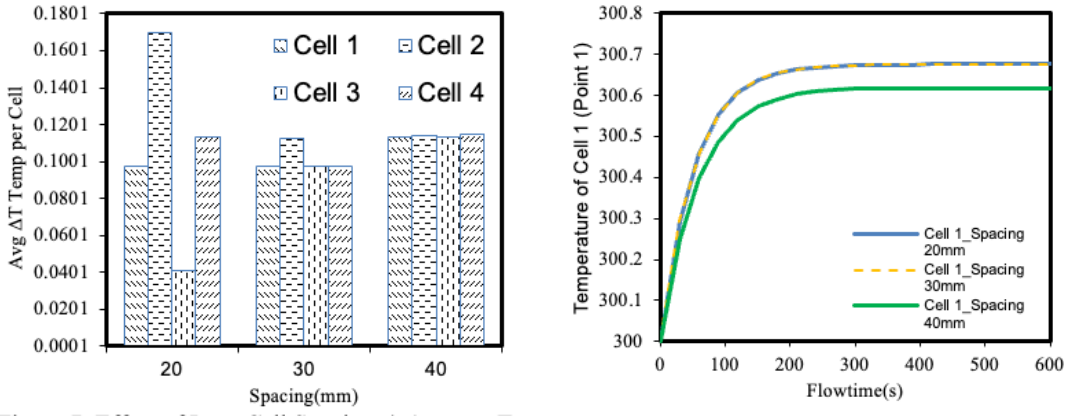

(a) **(b)**

Figure 9. Effect of Inter-Cell Spacing: **(a)** Average Temperature Difference versus Spacing and **(b)** Maximum Temperature versus Time.

Figure 9 (a) shows the average ΔT per cell across three different spacings (20, 30, and 40 mm). The ΔT values represent the difference between the maximum and minimum temperature within each cell, reflecting the uniformity of cooling. At 20 mm spacing, the ΔT is the highest, particularly for Cell 2. The smaller spacing leads to higher thermal gradients, causing localised heating and potential overheating in certain areas. This indicates poor thermal management, which can compromise battery safety and performance. At 30 mm spacing, the ΔT values are more balanced and moderate, suggesting improved cooling efficiency. The lower ΔT indicates a more uniform temperature distribution across the cells, reducing the likelihood of thermal hotspots and improving battery efficiency. For 40 mm spacing, the ΔT values are the lowest, confirming that larger spacing promotes the most effective cooling. The even thermal distribution across the cells minimises temperature fluctuations, ensuring consistent performance and increased battery lifespan.

Figure 9 (b) illustrates how the temperature of Cell 1 changes over time for different spacing configurations (20, 30, and 40 mm). The temperature increase is plotted against flowtime, with 20 mm spacing showing the fastest rise in temperature. The temperature stabilises at approximately 300.7 K after 600 s, indicating insufficient heat dissipation in this configuration. The close spacing restricts coolant flow, leading to localised overheating. In contrast, the 30 mm spacing leads to a more gradual temperature rise, stabilising at 300.62 K. This moderate spacing allows for better heat distribution, improving thermal efficiency. The slow rise indicates improved coolant circulation, reducing the chances of thermal degradation. The 40 mm spacing shows the slowest temperature increase, also stabilising at 300.62 K. The wider spacing facilitates optimal coolant flow, promoting more effective heat dissipation. This configuration offers the best thermal management, ensuring a more uniform temperature across the battery cells, reducing thermal stress, and enhancing battery life.

3.3.1. Optimal Thermal Parameters

Table 10 summarises the findings of this study and the ideal thermal management parameters. A coolant mixture containing 40% EG was identified as the most effective working fluid, providing efficient heat transfer. The optimal casing thickness was determined to be 1.5 mm, ensuring adequate heat dissipation; further increases in thickness beyond 2.0 mm did not yield significant improvements. An inter-cell spacing of 40 mm was found to enhance coolant circulation and promote temperature uniformity, thereby reducing thermal gradients between cells. Under these conditions, the maximum cell temperature was maintained below 313.00 K, which is within the safe operational limit. Additionally, the temperature variation between cells was minimised to less than 0.12 K, ensuring uniform temperature distribution across all cells. Collectively, these findings indicate that the proposed design parameters

provide efficient thermal regulation, enhance battery safety, and contribute to improved long-term performance and durability.

Table 10. Optimal Thermal Design Parameters and Their Performance Implications.

Parameter	Optimal Value	Remarks
Coolant Type	40% EG	Good efficiency
Casing Thickness	1.5 mm	Demonstrates effective heat dissipation; thicker casings (greater than 2.0 mm) did not significantly enhance performance
Inter-Cell Spacing	40 mm	Larger spacing promotes fluid circulation and temperature uniformity, thereby reducing the thermal gradient between cells
Maximum Temperature	<313.00 K	Within the safe operating temperature limit
ΔT between Cells	≤0.12 K	A low ΔT ensures uniform temperatures across all cells, leading to consistent efficiency and durability

The studies reported in this section emphasise the interdependence of coolant properties, geometric design, and flow parameters in achieving stable and uniform cooling performance. Further work is proposed in the following section to address model improvements and broaden the research focus.

4. Limitations and Future Work

Despite the useful insights gained from the study, several limitations must be addressed to provide a comprehensive understanding of the scope and relevance of the findings.

4.1. Study Limitations

This computational study was performed under a set of simplifying assumptions aimed at isolating the primary effects of casing thickness, inter-cell spacing, and coolant type on thermal behavior. For instance, coolant properties were considered constant regardless of temperature, which simplifies the modeling framework while providing clear insights into thermal trends. Although variations in density, viscosity, and thermal conductivity with temperature could influence heat transfer characteristics at higher temperatures, the present approach effectively highlights the core thermal interactions. The study used a single coolant flow rate of 0.005 kg/s and an inlet temperature of 298.00 K, reflecting typical conditions in automotive applications and providing a relevant baseline for performance evaluation across standard operational scenarios.

The model focused on a compact four-cell module, which allows detailed analysis of thermal responses while maintaining computational efficiency. While this geometry does not capture all complexities of a full battery pack, it offers foundational understanding applicable to larger-scale systems. Although experimental validation was not included, the numerical predictions furnish valuable qualitative insights into parameter influences and thermal trends that can guide future experimental studies. Lastly, the analysis concentrated on steady-state conditions to establish baseline thermal behavior, providing a necessary foundation for subsequent investigations into transient phenomena such as rapid charging and dynamic load cycles. Overall, the findings contribute important knowledge for battery thermal management design, supporting optimized parameter selection in electric vehicle and energy storage applications.

4.2. Future Research Directions

Building upon the findings of this study, future research should incorporate temperature-dependent properties of the coolant and cell materials to enhance simulation accuracy under real-world conditions. A comprehensive sensitivity analysis covering variations in flow rate, inlet temperature, and coolant composition would help identify optimal operating parameters. Extending the model to larger battery modules would allow evaluation of cooling performance and temperature uniformity at system scale, while experimental validation using prototype setups would strengthen model reliability. Additionally, investigating transient thermal behaviors during charging and discharging cycles and exploring hybrid cooling approaches, such as combining immersion and indirect liquid cooling or integrating phase-change materials, could further improve thermal management efficiency and safety. The current work

provides a solid foundation and modeling framework that supports these advancements toward practical and effective battery thermal management solutions.

5. Conclusion

This study examined the effects of coolant type, casing thickness, and inter-cell spacing on the thermal management of $LiFePO_4$ battery packs in relation to various cooling systems. The main findings indicate that, compared to pure water, a 40% EG–water mixture offers better cooling performance with practical applicability. An aluminium casing of 1.5 mm thick offers the best balance between heat dissipation and structural integrity. The study found minimal significant performance improvements at greater thicknesses, highlighting the importance of balancing cooling efficiency and material costs when designing batteries. Thermal performance was also shown to be significantly influenced by inter-cell spacing. The most uniform temperature distribution across the cells and the reduction of thermal gradients were obtained through the ideal fluid circulation achieved using a 40 mm spacing. By preventing localised overheating, this arrangement improves the battery's overall longevity and safety.

Although a 40 mm cell spacing showed the best thermal performance, as shown by the lowest average temperature differences and the smallest variation of ΔT between cells, this arrangement requires a significantly larger physical area. A balance between thermal efficiency and space limit must be considered in real-world applications where compactness and energy density are crucial, such as in portable systems or electric vehicles. Consequently, while 40 mm spacing provides optimum cooling, a 30 mm spacing may be more practical, allowing for increased packing density and improved volumetric efficiency, while still providing acceptable thermal performance. The findings of this study highlight the importance of selecting the ideal coolant, casing thickness, and spacing arrangement to ensure effective thermal management. With these ideal configurations, the battery pack may operate safely, effectively, and reliably by maintaining a maximum temperature below 313.00 K and achieving a moderate ΔT between cells. Maintaining temperature stability is essential for the functionality and longevity of battery-powered applications, and this research provides important insights for future battery system designs.

Author Contributions

Awangku Muhammad Dzul Hisyam: formal analysis, investigation, methodology, writing-original draft; Fauziah Jerai: supervision, conceptualisation, methodology, validation, writing-review and editing, resources; Nor Afifah Yahaya: conceptualisation, reviewing and editing; Norhayati Mat Wajid: reviewing and editing. All authors have read and agreed to the published version of the manuscript.

Funding

The authors acknowledge the Faculty of Mechanical Engineering, Universiti Teknologi MARA (UiTM), Malaysia, for providing access to the ANSYS Fluent software license used in this research.

Conflict of Interest Statement

The authors agree that this research was conducted in the absence of any self-benefits, commercial, or financial conflicts and declare the absence of conflicting interests with the funders.

Data Availability Statement

The data that support the findings of this study are not publicly available due to ethical restrictions.

Acknowledgment

This paper's publication fee is partially supported by the World Society of Sustainable Energy Technologies (WSSET) and the Faculty of Mechanical Engineering, Universiti Teknologi MARA (UiTM), Malaysia. The authors would also like to express their appreciation to previous final year project students under the Sustainable Energy Group for their contributions to the CFD work.

References

Aydin, D., Jarimi, H., Yuksel, B., Utlu, Z. & Riffat, S. (2025). Experimental investigation of a vertical flow moving bed thermochemical heat storage. Energy Catalyst, 1(5), 68–78. https://doi.org/10.61552/EC.2025.005.

Al-Baghdadi, M.A.R.S. (2020). Can CFD analysis help PEM fuel cell design and operation? OPAL (Open@LaTrobe). https://doi.org/10.32545/encyclopedia202004.0023.v1.

Dambros Telli, G., Gungor, S. & Lorente, S. (2024). Counterflow solutions for battery modules. Applied Thermal Engineering, 238, 121997. https://doi.org/10.1016/j.applthermaleng.2023.121997.

Duan, J. et al. (2021). Heat dissipation modelling for liquid cooling lithium-ion batteries. Energies, 14(14), 4187. https://doi.org/10.3390/en14144187.

Gundran, J.E.M., Ubando, A.T. & Culaba, A.B. (2019). Investigation of the thermal performance of a wavy channel liquid cooling system for EV batteries. https://doi.org/10.1109/hnicem48295.2019.9072774.

Guo, Z. et al. (2022). Multichannel direct contact liquid cooling system. IEEE Transactions on Transportation Electrification, 8(2), 2334–2345. https://doi.org/10.1109/tte.2021.3131718.
Hemavathi, S. et al. (2024). Temperature distribution in fast-discharging Li-ion battery pack. Heat Transfer Research, 55(2), 41–54. https://doi.org/10.1615/heattransres.2023048880.
Idris, M.S. & Zakaria, I.A. (2024). Water:EG properties with Al_2O_3 & SiO_2 nanoparticles. Journal of Mechanical Engineering, 21(1), 255–277. https://doi.org/10.24191/jmeche.v21i1.25371.
Jarimi, H., Devrim, A., Su, Y. & Riffat, S. (2025). Controllable supercooling in phase change materials: Advances in triggering methods, lab-scale investigations and prototype demonstrations. Global Decarbonisation Journal, 1–25. https://doi.org/10.17184/eac.9501.
Lan, C., Xu, J., Qiao, Y. & Ma, Y. (2016). Thermal management for high power lithium-ion battery by minichannel aluminium tubes. Applied Thermal Engineering, 101, 284–292. https://doi.org/10.1016/j.applthermaleng.2016.02.070.
Lin, J., Liu, X., Li, S., Zhang, C. & Yang, S. (2021). A review on recent progress, challenges and perspectives of battery thermal management systems. International Journal of Heat and Mass Transfer, 167, 120834. https://doi.org/10.1016/j.ijheatmasstransfer.2020.120834.
Liu, Z., Liu, X., Meng, H., Guo, L. & Zhang, Z. (2021). Numerical analysis of liquid cooling battery module. International Journal of Heat and Mass Transfer, 175, 121338. https://doi.org/10.1016/j.ijheatmasstransfer.2021.121338.
Liu, J., Ma, Q. & Li, X. (2023). Immersion cooling performance of Li-ion battery module. Journal of Energy Storage, 66, 107511. https://doi.org/10.1016/j.est.2023.107511.
Omar, A.A. & Adham, A.M. (2025). Thermal analysis of Li-ion batteries using forced-air cooling. International Journal of Thermofluids, 101212. https://doi.org/10.1016/j.ijft.2025.101212.
Riffat, J., Doudran, H.A. & Samaei, S.R. (2025). AI-enhanced damage detection in jack-up rig legs using an improved modal strain energy index: A numerical, experimental, and digital twin-based approach. Green Technology & Innovation, 25, 340014. https://doi.org/10.36922/GTI025340014.
Richardson, G., Foster, J.M., Ranom, R., Please, C.P. & Ramos, Á. (2021). Charge transport modelling of lithium-ion batteries. European Journal of Applied Mathematics, 33(6), 983–1031. https://doi.org/10.1017/S0956792521000292.
Situ, W. et al. (2017). Thermal management system using mesh-enhanced PCM plates. Energy, 141, 613–623. https://doi.org/10.1016/j.energy.2017.09.083.
Sirikasemsuk, S., Wiriyasart, S., Prurapark, R., Naphon, N. & Naphon, P. (2021a). Water/nanofluid pulsating flow in thermoelectric module. International Journal of Heat and Technology, 39(5), 1618–1626. https://doi.org/10.18280/ijht.390525.
Sirikasemsuk, S., Wiriyasart, S., Naphon, P. & Naphon, N. (2021b). Thermoelectric ferrofluid BTMS. International Journal of Energy Research, 45, 8824–8836. https://doi.org/10.1002/er.6417.
Syam Sundar, L. & Shaik, F. (2023). Heat transfer and exergy efficiency of nanofluids. International Journal of Thermal Sciences, 184, 107901. https://doi.org/10.1016/j.ijthermalsci.2022.107901.
Wang, J., Lv, J., Lin, W., Song, W. & Feng, Z. (2024). Heat generation rate estimation of Li-ion batteries. Applied Thermal Engineering, 123752. https://doi.org/10.1016/j.applthermaleng.2024.123752.
Wang, H., Tao, T., Xu, J., Mei, X., Liu, X. & Gou, P. (2020). Cooling capacity of a novel modular liquid-cooled BTMS. Applied Thermal Engineering, 178, 115591. https://doi.org/10.1016/j.applthermaleng.2020.115591.
Xu, H., Zhang, X., Xiang, G. & Li, H. (2021a). Optimization of liquid cooling of Li-ion packs. Case Studies in Thermal Engineering, 26, 101012. https://doi.org/10.1016/j.csite.2021.101012.
Xu, Y., Li, X., Liu, X., Wang, Y., Wu, X. & Zhou, D. (2021b). Composite silica gel plate with liquid cooling for battery thermal management. Applied Thermal Engineering, 184, 116217. https://doi.org/10.1016/j.applthermaleng.2020.116217.
Zeng, Y. & Bazant, M.Z. (2014). Phase separation dynamics in isotropic ion-intercalation particles. SIAM Journal on Applied Mathematics, 74(4), 980–1004. https://doi.org/10.1137/130937548.
Zhang, G. et al. (2023). Lithium iron phosphate and layered transition metal oxide cathodes for power batteries. Materials, 16(17), 5769. https://doi.org/10.3390/ma16175769.
Zhao, D., Lei, Z. & An, C. (2023). Liquid cooling plate with honeycomb-like flow channel. Applied Thermal Engineering, 218, 119324. https://doi.org/10.1016/j.applthermaleng.2022.119324